Cu adatom interactions with single- and polycrystalline $Bi_2Ca_{1+x}Sr_{2-x}Cu_2O_{8+y}$ and $YBa_2Cu_3O_{7-x}$

D. M. Hill, H. M. Meyer III, and J. H. Weaver
Department of Chemical Engineering and Materials Science, University of Minnesota, Minneapolis, Minnesota 55455

C. F. Gallo
3M Center, Building 201-1E, St. Paul, Minnesota 55144

K. C. Goretta
Argonne National Laboratory, Argonne, Illinois 60439
(Received 11 July 1988)

The electronic structure and surface interactions of vapor-deposited Cu on single-crystal and polycrystalline $Bi_2Ca_{1+x}Sr_{2-x}Cu_2O_{8+y}$ were studied using x-ray photoelectron spectroscopy. The results are compared to the Cu/$YBa_2Cu_3O_{7-x}$ interface. Changes in the Cu $2p$ satellite emission indicate that the Cu adatoms do not disrupt $Bi_2Ca_{1+x}Sr_{2-x}Cu_2O_{8+y}$ as extensively as $YBa_2Cu_3O_{7-x}$. However, deposition of Cu induces changes in the Bi environment in the superconductor, and surface segregation of Bi metal was observed at high coverages. Core-level attenuation results suggest minimal out-diffusion of oxygen, in contrast with what is observed for Cu/$YBa_2Cu_3O_{7-x}$.

INTRODUCTION

The recent synthesis[1,2] of Bi-Ca-Sr and Tl-Ca-Ba copper oxides with superconducting transition temperatures T_c greater than 110 K has raised important questions about their chemical properties relative to those of the rare-earth copper oxide superconductors. It is now well known that surfaces of the high-T_c superconductors of 2:1:4 and 1:2:3 stoichiometry are disrupted by the deposition of metal adatoms which have an affinity for oxygen.[3] For example, x-ray photoemission spectroscopy (XPS) results show that adatoms of Cu deposited on these materials react with and remove O from the superconductor, despite the low bulk heats of formation of copper oxides relative to rare-earth oxides. This reaction reduces the nominal oxidation state of Cu within at least ~30–50 Å of the surface from Cu^{2+} to Cu^{1+}, disrupts the crystal structure, and undoubtedly destroys superconductivity in this region. Analogous behavior has been found during deposition of the metals Ti, Fe, Pd, La, Al, and In, as well as the semiconductor Ge. In contrast, Bi is much less reactive, and Ag and Au exhibit no tendency for reaction.

The purpose of this paper is to examine Cu interfaces on single-crystal and polycrystalline $Bi_2Ca_{1+x}Sr_{2-x}Cu_2O_{8+y}$ and to quantitatively compare the results with those obtained for Cu on $YBa_2Cu_3O_{7-x}$. Our x-ray photoemission studies of the effects of Cu adatoms evaporated at room temperature onto $Bi_2Ca_{1+x}Sr_{2-x}Cu_2O_{8+y}$ show reactions for both single- and polycrystalline surfaces. We find that the rate of attenuation of the Cu $2p$ satellites (which reflects the valence change) was less than for Cu on $YBa_2Cu_3O_{7-x}$. This suggests that the Bi-based superconductors are intrinsically more stable. However, analysis of the Bi $4f$ core-level results also indicates changes in Bi bonding induced by Cu adatoms. This, plus the ultimate segregation of Bi atoms to the surface of the growing Cu layer, implies that the Cu adatoms also disrupt the Bi-O planes.

EXPERIMENTAL TECHNIQUES

X-ray photoelectron spectroscopy measurements of interface formation were performed under standard ultrahigh vacuum conditions (pressure during measurement less than 1×10^{-10} Torr). A monochromatic beam of Al $K\alpha$ photons ($h\nu=1486.6$ eV) was focused on the sample surface and the energy of the emitted electrons was measured with a Surface Science Instruments hemispherical analyzer using a resistive anode position-sensitive detector. The photoelectrons were collected at an angle of 60° relative to the surface normal and the cone of acceptance of the analyzer was 30°. The x-ray beam diameter was 300 μm at the sample and the pass energy of the analyzer was 50 eV. The Cu $2p_{3/2}$ emission from pure Cu was used to calibrate the binding-energy scale (binding energy of 932.5 eV). Data were acquired and analyzed on a dedicated HP9836C computer. Core-level binding-energy shifts and the attenuation of the substrate core-level emission as a function of overlayer thickness were used to identify reacting species and overlayer growth morphology. Although representative spectra are shown in the figures, the evolution of the interfaces were examined for depositions of 0.5, 1, 2, 4, 8, 16, 30, 40, 50, and 80 Å of Cu.

The single-crystal samples ($2\times2\times0.5$ mm^3) were extracted from a eutectic melt of constituent powders and were then annealed in O_2/air at 780 °C. The resulting crystals exhibited superconductivity at 85 K as measured by magnetic susceptibility. The sintered material was synthesized from a melt of Bi_2O_3, $SrCO_3$, CaO, and CuO, splat quenched on a chilled copper plate, and then annealed in O_2/air. This also resulted in material that was

superconducting at 85 K, as determined by resistivity measurements. The polycrystalline $YBa_2Cu_3O_{7-x}$ sample was synthesized from a stoichiometric mix of CuO, Y_2O_3, and Ba_2CO_3 and subjected to several annealing cycles to give the desired phase. The transition temperature of the resulting material was ~93 K. The samples were cleaved (or fractured in the case of the sintered material) *in situ* immediately before the measurements. *In situ* optical examination of the cleaved single-crystal surfaces showed planar, mirrorlike regions as well as rough areas with many steps and terraces for the single crystals. Both types of surface could be probed separately with the 300-μm photon beam and only minor differences in the core-level and valence-band features were observed. Fracturing the polycrystalline $Bi_2Ca_{1+x}Sr_{2-x}Cu_2O_{8+y}$ samples exposed rough, granular internal surfaces, suggesting that a large fraction of the surface was due to intergranular fracture. Scanning electron microscopy (SEM) of these surfaces showed both needlelike ($\sim 1\times 1\times 20$ μm) and platelike ($\sim 1\times 15\times 15$ μm) grains. Large voids were also found ($\sim 50-100$ μm). The needlelike grains were localized on interior surfaces of the voids and the platelike grains were found on internal surfaces. The planar grains showed both intergranular (~75%) and transgranular (~25%) fracture surfaces, confirming the results of optical microscopy. The transgranular fracture surfaces were similar to the rough areas observed for the single-crystal samples, although on a much smaller scale. A negligibly small fraction of the needlelike grains were fractured. SEM micrographs of the $YBa_2Cu_3O_{7-x}$ surfaces showed a higher proportion (~80%) of transgranular fracture, and a generally smoother surface morphology.

Adatoms of Cu were evaporated from resistively heated W baskets and deposited onto the freshly prepared surfaces. The source-to-sample distance was ~30 cm and typical evaporation rates were ~1 Å/min. The amount of metal deposited was measured with an Inficon quartz crystal oscillator. The pressure in the chamber was kept below 2×10^{-10} Torr during evaporation.

For each of the interfaces studied, the XPS energy distribution curves (EDC's) were measured for the valence bands and the Cu 2*p* and O 1*s* core levels, as well as Bi 4*f*, Ca 2*p*, Sr 3*d*, Y 3*d*, and Ba 3*d*, as appropriate. The core-level spectra were fit with Gaussian and convolved Gaussian and Lorentzian functions to determine the binding energy, peak width, and integrated intensity of each feature at each stage of interface formation. S-shaped background functions were subtracted prior to fitting.

RESULTS AND DISCUSSION

Clean surfaces of $Bi_2Ca_{1+x}Sr_{2-x}Cu_2O_{8+y}$

Figure 1 shows the valence bands and shallow core-level emission for $Bi_2Ca_{1+x}Sr_{2-x}Cu_2O_{8+y}$ within 44 eV of the Fermi level, E_F. The solid line shows the results for the single crystal and the dashed line reveals differences associated with the polycrystalline samples. The broad feature with a maximum ~3.4 eV below E_F is primarily due to emission from Cu–O hybrid bonds, with small contributions from Bi–O hybrids and O 2*p* levels, as shown in recent band-structure calculations.[4–6] Emission

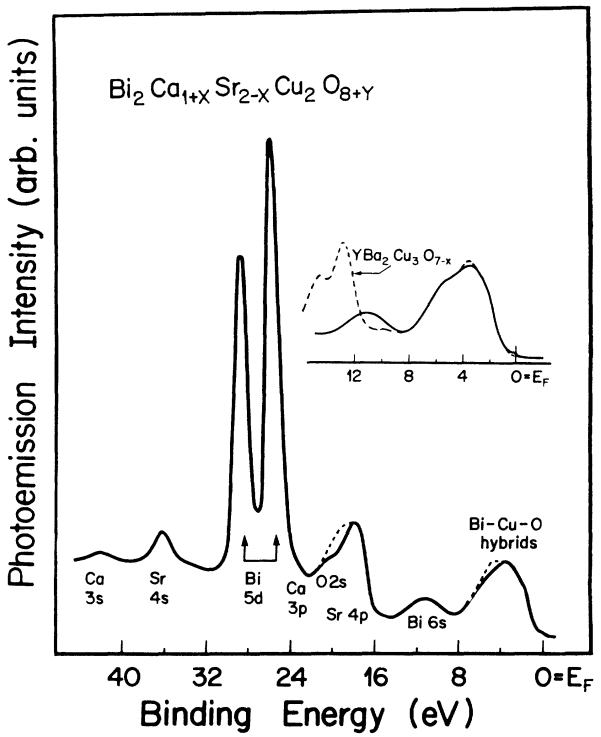

FIG. 1. Valence-band and shallow core-level emission for single-crystal (solid line) and polycrystalline (dashed line) $Bi_2Ca_{1+x}Sr_{2-x}Cu_2O_{8+y}$. The inset compares the valence bands for the single crystal with those measured for $YBa_2Cu_3O_{7-x}$, and shows the similarities due to the Cu–O hybrid states and the enhanced emission at the Fermi level for $Bi_2Ca_{1+x}Sr_{2-x}Cu_2O_{8+y}$.

from both types of samples had shoulders at 2.1 and 5.4 eV, with the polycrystalline sample exhibiting proportionately more emission at 5.4 eV. This is consistent with the presence of impurity phases, probably at grain boundaries, and has been observed for other polycrystalline high-T_c superconductors.[3] In the inset of Fig. 1 we compare the valence-band emission for single-crystal $Bi_2Ca_{1+x}Sr_{2-x}Cu_2O_{8+y}$ to that of $YBa_2Cu_3O_{7-x}$ (dashed line). That comparison shows that the 2:1:2:2 materials have slightly greater emission intensity at the Fermi level and slightly less at ~3.4 eV. These differences notwithstanding, it is clear that the general shape of the valence-band emission for these 2:1:2:2 materials is very similar to those observed for the 2:1:4- and 1:2:3-type superconductors, again consistent with dominant Cu–O bonding in each case and the same kind of correlation effects.

The structure at ~11.3 eV is due to the broad, quasicore Bi 6*s* emission. Its presence in these 2:1:2:2 materials masks features which have been observed in the other superconductors and which should be expected here, namely the Cu d^8 satellite at ~12 eV and the feature near 9 eV. As labeled, the Ca 3*s* emission appears at 42.3 eV and the Sr 4*s* emission is at 36.2 eV. The O 2*s* and the Sr 4*p* features overlap at ~19 eV, and this structure is broader in the polycrystalline sample (dashed line). As will be discussed below with respect to the Sr 3*d* core level, this broadening is due to a second Sr component on the

high-binding-energy side. The Ca $3p$ emission appears as a slight shoulder on the low-binding-energy side of the intense Bi $5d$ doublet. We note here that all of the core-level and valence-band features were stable in time and reproducible from cleave to cleave.

In Fig. 2 we show representative core-level spectra obtained for single-crystal (left column) and polycrystalline (right column) samples of $Bi_2Ca_{1+x}Sr_{2-x}Cu_2O_{8+y}$. The O $1s$ spectrum for the single crystal shows a single, relatively broad peak centered at 528.8 eV [full width at half maximum (FWHM) of 1.6 eV] with a very small shoulder near 531 eV. Detailed examination of the main feature suggests that there are at least three components, corresponding to O atoms in Cu-O planes, Bi-O planes, and in off-plane sites bonded to the alkali earths and Bi. Unfortunately, fits using a contribution from each of these environments are not unique. From the O $1s$ spectra shown at the top of Fig. 2, it is also clear that the polycrystalline samples exhibit chemical configurations for O that are not present for the single crystals. We associate them with extrinsic effects due to grain-boundary phases and not intrinsic properties of the superconductor, analogous to results for the 1:2:3 and 2:1:4 materials where structure at ~531 eV was associated with contamination.[3,7] For the 2:1:2:2 polycrystalline sample ~20% of the total emission intensity can be associated with the nonsuperconducting phases. (It is important to note that emission from any grain-boundary phases exposed by fracture is enhanced by the surface sensitivity of the XPS technique. The fraction of signal due to impurities is thus an upper limit to the impurity of the sample.) Finally, we note that the main O $1s$ emission peak for the polycrystalline samples was wider, FWHM ~2 eV, and had a more pronounced shoulder on the low-binding-energy side. Comparison of the core-level intensities for Bi, Ca, Sr, and Cu revealed that the polycrystalline sample had proportionally more Ca, which suggests that this feature is due to O coordinated with Ca atoms. Since the shoulder was also present in the single-crystal sample, which had minimal amounts of the cantaminant phases, it is likely to be intrinsic to the superconducting phase.

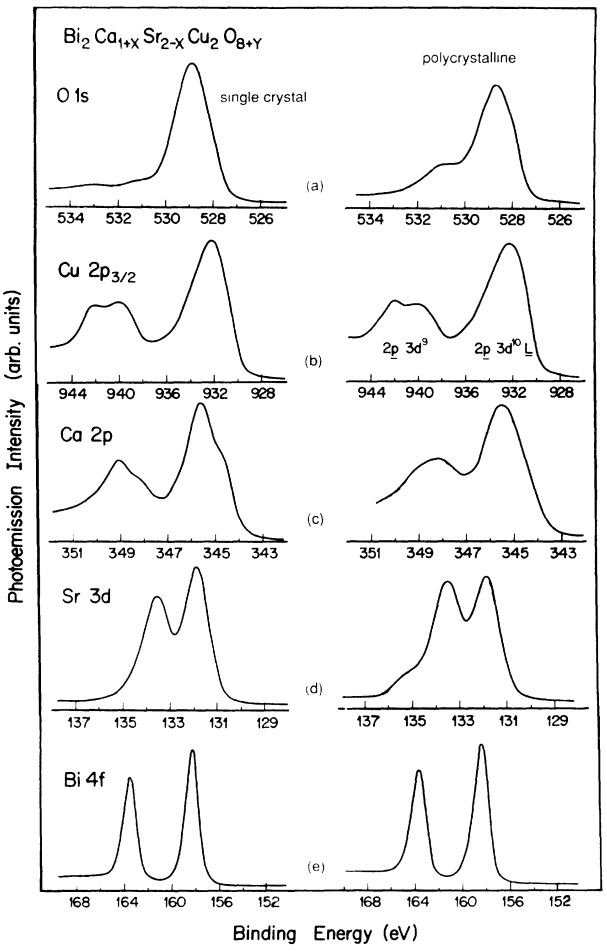

FIG. 2. Core-level spectra for single-crystal (left column) and polycrystalline (right column) $Bi_2Ca_{1+x}Sr_{2-x}Cu_2O_{8+y}$, showing the differences between the O $1s$, Ca $2p$, and Sr $3d$ chemical environments, and the apparent single-bonding configurations of Cu and Bi.

The Cu $2p_{3/2}$ emission shown in Fig. 2 is typical of all of the high-T_c superconductors with a broad, main peak centered at ~933 eV (Cu $2\underline{p}_{3/2}3d^{10}\underline{L}$ final-state configuration) and a double-peaked satellite structure between 939 and 943 eV (multiplet states of the $2\underline{p}_{3/2}3d^9$ configuration). The origin of these features for other high-T_c superconductors and CuO has been discussed in detail elsewhere.[8] For $Bi_2Ca_{1+x}Sr_{2-x}Cu_2O_{8+y}$, the Cu $2p_{3/2}$ emission is complicated somewhat by overlapping Bi $4s$ emission at ~938.5 eV. The Bi $4s$ is broad (~9 eV FWHM as determined from spectra of oxidized Bi), and its photoionization cross section is ~10% of that of the Cu $2p_{3/2}$ emission.[9] Nonetheless, it causes the apparent increase in the background beneath the Cu $2p_{3/2}$ emission, relative to that for $YBa_2Cu_3O_{7-x}$. The satellite intensity also appears greater than for the other superconductors, again due to the underlying Bi $4s$ emission (39% of the main peak intensity for the single-crystal sample compared to 34% for $YBa_2Cu_3O_{7-x}$). The shapes of the Cu $2p$ satellite emission shown for the single-crystal and polycrystalline samples are qualitatively the same, but there are different intensities of the predominant peaks on either side. The differences are most likely due to a combination of two effects: the slightly different amounts of Bi in the samples (~10% more in the single-crystal sample) and the different oxidation states of Bi in the polycrystalline sample, as discussed below.

The Ca $2p$ and Sr $3d$ core-level results shown in Fig. 2 reveal the intrinsic superconductor emission as well as contributions from the impurity phases. Line-shape analysis for the single-crystal, clean-surface results for both Ca and Sr shows two spin-orbit-split pairs. For Sr, the $3d$ doublets are shifted 1.35 eV and the intensity of the shallower doublet exceeds that of the deeper pair by a factor of 2.4. For Ca, the splitting can be easily seen from the raw data, with the $2p_{3/2}$ features appearing at 344.7 and 345.6 eV and the deeper doublet being larger by a factor of 1.28. These Ca and Sr core-level binding energies are *lower* than for the elements in their metallic state. This is in contrast to shifts toward *higher* binding energies which have been observed for CaO (~1.25 eV for the Ca $2p_{1/2,3/2}$ peaks) and SrO (~0.8 eV for Sr $3d_{3/2,5/2}$).[10] In

particular, the main Sr $3d_{5/2}$ emission in 2:1:2:2 appears at 131.8 eV, much less than the 134.2 eV measured for metallic Sr. The center of the Ca $2p_{3/2}$ emission was measured at 345.1 eV binding energy, which is lower than all previously reported values for metallic Ca [which range from 345.7 to 347 eV (Ref. 10)]. We associate the shallower features with atoms in the dimpled alkali-metal oxygen planes between Bi-O and Cu-O planes while the deeper structure corresponds to the intercalated layer between Cu-O planes. For the single crystals, the ratio of the two components for Ca and Sr also varied somewhat from sample to sample, consistent with variations in x in the formula unit and with Sr-Ca disorder, but the sum of the Ca and Sr emission was almost constant. The results of Fig. 2 for Ca $2p$ and Sr $3d$ emission from the polyscrystalline samples reveal significantly different line shapes and line-shape analysis is much less unique. Qualitatively, it can be seen that there is substantially increased emission at lower binding energy for the Ca $2p$ emission while a pronounced higher energy shoulder is evident for the Sr $3d$ emission. Based on the O $1s$ results, we suggest that these differences are due to impurity phases for the polycrystalline samples which distort the line shapes for the superconductor.

Finally, in the bottom panel of Fig. 2 we show the sharp Bi $4f_{5/2,7/2}$ emission with a slight asymmetry toward higher binding energy that is consistent with metallic screening. For the polycrystalline samples, the linewidths were broader, suggesting some inequivalent bonding configurations, but the effects are much less evident than for Sr or Ca. Based on the large changes in binding energy observed during reduction of Bi (~1.5 eV, discussed below), this suggests that the grain boundaries contain relatively little Bi, not that the Bi $4f$ emission is insensitive to the chemical environment. We note that the measured Bi $4f_{5/2}$ and $4f_{7/2}$ binding energies of 163.5 and 158.2 eV for the 2:1:2:2 material are slightly smaller than those reported for Bi_2O_3 [163.8 and 158.5 eV (Ref. 11)], which may reflect the novel Bi chemical environment in these superconductors.

Cu/$Bi_2Ca_{1+x}Sr_{2-x}O_{8+y}$ and Cu/$YBa_2Cu_3O_{7-x}$ interfaces

In the following, we present XPS results obtained during the formation of Cu/$Bi_2Ca_{1+x}Sr_{2-x}Cu_2O_{8+y}$ interfaces and we compare them with results for Cu/$YBa_2Cu_3O_{7-x}$. We will not review the XPS spectra for clean surfaces of $YBa_2Cu_3O_{7-x}$ since they were presented in Ref. 3. Here, we are particularly concerned with the relative stability of the materials during interface formation because previous interface studies indicate that $Bi_2Ca_{1+x}Sr_{2-x}Cu_2O_{8+y}$ is more stable, perhaps due to the double layers of Bi-O.[12]

In Fig. 3 we show the Cu $2p_{3/2}$ core-level and satellite spectra obtained for representative Cu depositions on $YBa_2Cu_2O_{7-x}$ and on single-crystal $Bi_2Ca_{1+x}Sr_{2-x}Cu_2O_{8+y}$. The spectra are normalized to acquisition time and Cu content of the samples so that the heights of the satellite features quantitatively represent their relative intensities. The clean surface spectra (bottom curves) show subtle differences in shape for the main lines, satellites, and backgrounds. For both materials, the deposition of Cu leads to an abrupt loss of satellite intensity, indicating extensive reaction between the Cu adatoms and the substrate. The relative intensity of the satellite emission $YBa_2Cu_3O_{7-x}$ decreased to 37% of its original value by 1-Å-Cu deposition, compared to 67% for single-crystal $Bi_2Ca_{1+x}Sr_{2-x}Cu_2O_{8+y}$. Furthermore, for Cu/$YBa_2Cu_3O_{7-x}$ the satellite structure characteristic of the Cu^{1+} state[9] appeared at 1.5 Å of Cu coverage, i.e., enhanced emission at ~944 eV and reduced emission at ~940 eV. In contrast, the same changes in satellite structure were not observed until 4-Å Cu coverage for the single-crystal

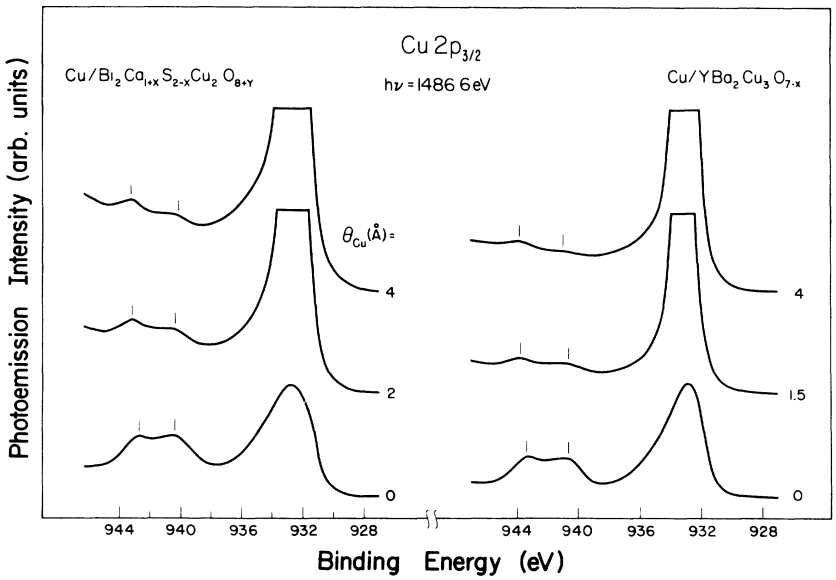

FIG. 3. Cu $2p_{3/2}$ satellite emission from $YBa_2Cu_3O_{7-x}$ (left column) and $Bi_2Ca_{1+x}Sr_{2-x}Cu_2O_{8+y}$ (right column) as a function of Cu coverage, showing the more rapid attenuation of the satellite intensity for the 1:2:3 material.

$Bi_2Ca_{1+x}Sr_{2-x}Cu_2O_{8+y}$ interface. For the polycrystalline sample of $Bi_2Ca_{1+x}Sr_{2-x}Cu_2O_{8+y}$, the net attenuation of the satellite intensity was even less than for the single crystal for the same Cu coverage, and the satellite structure characteristic of Cu^{2+} persisted to ~16-Å Cu coverage.

The persistence of the 2+ Cu configuration for the polycrystalline sample is probably a consequence of the irregular morphology of the substrate. In particular, the fractured surface of the polycrystalline sample was much rougher than either the single crystal or the sintered $YBa_2Cu_3O_{7-x}$ sample. As a result, there is non-negligible shadowing of the probed surface from the evaporator. Indeed, for these experiments the Cu was evaporated onto the surface at normal incidence and the collection angle of the photoemitted electrons was 60° relative to the surface normal. This clearly results in uneven deposition of adatoms, with some probed regions receiving none, as was confirmed by examining line-shape changes as a function of emission angle. Although the $YBa_2Cu_3O_{7-x}$ sample is also sintered, the effects of surface morphology are greatly reduced because the fractured surface is smoother than $Bi_2Ca_{1+x}Sr_{2-x}Cu_2O_{8+y}$ and there is a larger amount of transgranular fracture.

The O 1*s* emission from the 2:1:2:2 material (not shown) is also affected by Cu deposition. In particular, the deposition of 0.5 Å caused a shift in centroid of 0.35 and 0.25 eV for single-crystal and sintered samples, respectively, with negligible subsequent changes. This is compared to 0.3 eV for the same Cu coverage on $YBa_2Cu_3O_{7-x}$ where subsequent depositions caused a total shift of 0.75 eV. In addition, for the single crystal the attenuation of the O 1*s* signal was approximately exponential with Cu coverage and there was no evidence of the sort of O out-diffusion that was observed for $YBa_2Cu_3O_{7-x}$ (Ref. 3). For the sintered 2:1:2:2 sample, the absolute magnitudes of attenuation were complicated by morphological effects, but the relative ratios of the O 1*s* signal to the Sr and Ca emission were nearly the same, again suggesting that there was no O out-diffusion.

Analysis of the attenuation of the Sr 3*d* and Ca 2*p* core levels for the 2:1:2:2 single crystals also showed exponential behavior as a function of Cu coverage, implying negligible Sr or Ca out-diffusion or surface segregation and indicating that comparisons of the oxygen behavior to Sr or Ca are meaningful. For Cu coverages between 0.5 and 2 Å the Sr 3*d* and Ca 2*p* core-level spectra (not shown) both shifted ~0.4 eV to higher binding energy and small, high-binding-energy components grow at low coverage, contributing less than 15% of the total emission. Interestingly, these new features do not change during subsequent Cu deposition. In contrast, substantial changes were observed in the Y 3*d* and Ba $3d_{5/2}$ emission for the $Cu/YBa_2Cu_3O_{7-x}$ interface and Ba segregation was also documented. We conclude that Cu induces less disruption on the Bi-based superconductor than on the 1:2:3 and 2:1:4 materials.

Although the present results show that the 2:1:2:2 interface is less reactive than the other superconductors, they also provide clear evidence for chemical activity. Chemical interaction is confirmed by the results of Fig. 4 which show the evolving line shape for the Bi 4*f* levels for single-crystal and polycrystalline samples. The deposition of 0.5 Å of Cu induces a shift of 0.3 eV in the Bi 4*f* peak position to that measured for Bi_2O_3 (see tick marks). The 4*f* line shapes also broadened 0.4 eV for the single crystal

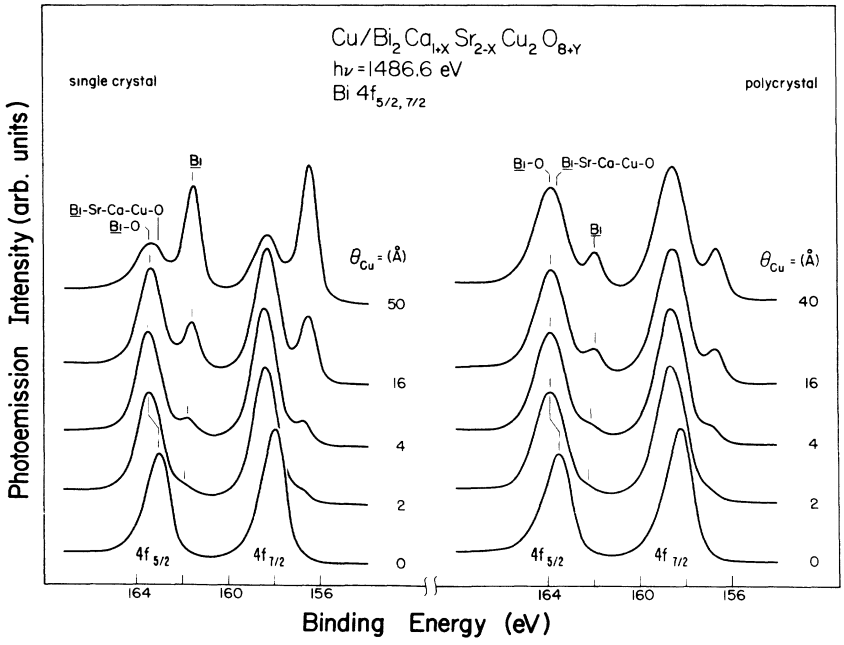

FIG. 4. Bi 4*f* emission as a function of Cu coverage for single-crystal (left column) and polycrystalline (right column) $Bi_2Ca_{1+x}Sr_{2-x}Cu_2O_{8+y}$ showing the initial binding-energy shift at low coverages, and then the growth of the segregating Bi signal on the low-binding-energy side.

and 0.2 eV for the sintered sample, indicating the disruption of Bi-O planes by the Cu adatoms and a variety of inequivalent chemical sites. These positions and widths then remained constant to coverages up to 16 Å. At the same time, a new Bi $4f$ feature appeared at lower binding energy by ~1-Å Cu deposition and then grew in absolute intensity until ~16 Å Cu for both surfaces. By ~8 Å Cu, the binding energies of these features had converged to 161.9 and 156.7 eV, which coincide with the energies measured for Bi metal.

Analysis of the intensity and rate of attenuation of the newly formed Bi feature shows that it attenuates at a much slower rate than the substrate-related component. This implies that these new Bi atoms are not spacially constrained to the buried interface but rather that there is Bi segregation on the growing Cu overlayer. The high-coverage results show that the intensity of this component is much smaller for the polycrystalline sample than for the single crystal (Fig. 4). This is partially due to morphological effects, as noted above. In addition, it appears that reactions with the grain-boundary phases differ from those with the 2:1:2:2 phase, and that it is only the latter that gives rise to Bi release into the overlayer.

SUMMARY

In this paper, we have shown that Cu adatoms react with and disrupt both single-crystal and polycrystalline samples of the high-T_c superconductor $Bi_2Ca_{1+x}Sr_{2-x}Cu_2O_{8+y}$, but to a lesser extent than has been observed for $YBa_2Cu_3O_{7-x}$. Polycrystalline samples were disrupted less for equal Cu coverages, despite the possible channels of attack through grain boundaries. This suggests that the grain-boundary phases inhibit reaction. For higher Cu coverages, segregation of Bi was observed. This may indicate a preferential interaction with the Bi-O planes. These results demonstrate that the 2:1:2:2 materials are more stable with respect to Cu-induced disruption, Cu-O formation, and the leaching of O from the substrate.

ACKNOWLEDGMENTS

The work at the University of Minnesota was supported by the Office of Naval Research and the Defense Advanced Research Projects Agency. That at Argonne National Laboratory was supported by the U.S. Department of Energy.

[1]C. Michel, M. Hervieu, M. M. Borel, A. Grandin, F. Deslandes, J. Provost, and B. Raveau, Z. Phys. B **68**, 421 (1987).

[2]H. Maeda, Y. Tanaka, M. Fukutomi, and T. Asano, Jpn. J. Appl. Phys. **27**, L209 (1988).

[3]H. M. Meyer III, D. M. Hill, T. J. Wagener, Y. Gao, J. H. Weaver, D. W. Capone II, and K. C. Goretta, Phys. Rev. B **38**, 6500 (1988) and references therein for characterization of 1:2:3 superconductors. For 2:1:2:2 results, see H. M. Meyer III, D. M. Hill, J. H. Weaver, D. L. Nelson, and C. F. Gallo, Phys. Rev. B **38**, 7144 (1988); A. Fujimori, S. Takekawa, E. Takayama-Moromachi, Y. Uchida, A. Ono, T. Takahashi, Y. Okabe, and H. Katayana-Yoshida (unpublished); M. Onellion, M. Tang, Y. Chang, G. Margaritondo, J. M. Tarascon, P. A. Morris, W.A. Bonner, and N. G. Stoffel, Phys. Rev. B **38**, 881 (1988).

[4]S. Massidda, J. Yu, and A. J. Freeman, Physica C **152**, 251 (1988); P. Marksteiner, S. Massidda, Jaejun Yu, A. J. Freeman, and J. Redinger, Phys. Rev. B **38**, 5098 (1988).

[5]H. Krakauer and W. E. Pickett, Phys. Rev. Lett. **60**, 1665 (1988).

[6]M. S. Hybersten and L. F. Mattheiss, Phys. Rev. Lett. **60**, 1661 (1988).

[7]J. H. Weaver, H. M. Meyer III, T. J. Wagener, D. M. Hill, Y. Gao, D. Peterson, Z. Fisk, and A. J. Arko, Phys. Rev. B **38**, 4668 (1988), discuss results for single crystals of 1:2:3 and 2:1:4 superconductors, with particularly detailed line-shape analysis for the O 1s spectra.

[8]G. van der Laan, C. Westra, C. Haas, and G. A. Sawatsky, Phys. Rev. B **23**, 4369 (1981).

[9]J. H. Scofield, J. Electron. Spectrosc. Relat. Phenom. **8**, 129 (1976).

[10]H. van Doveren and J. A. Verhoeven, J. Electron. Spectrosc. Relat. Phenom. **21**, 265 (1980), and references therein.

[11]T. P. Debies and J. W. Rablais, Chem. Phys. **20**, 277 (1977).

[12]H. M. Meyer III, D. M. Hill, J. H. Weaver, D. L. Nelson, and K. C. Goretta [Appl. Phys. Lett. **53**, 1004 (1988)] compare reactions and passivation for Bi overlayers on $YBa_2Cu_3O_{7-x}$ and $Bi_2Ca_{1+x}Sr_{2-x}Cu_2O_{8+y}$. Surface passivation is also discussed in D. M. Hill, H. M. Meyer III, J. H. Weaver, and D. L. Nelson, Appl. Phys. Lett. **53**, 1657 (1988).